sustainability

MDPI

Article

Effect of Freeze–Thaw Cycles on the Microstructure Characteristics of Unsaturated Expansive Soil

Xinyu Li [1,2], Shengyi Cong [1,2,3,*], Liang Tang [1,2,3] and Xianzhang Ling [1,2,3]

[1] School of Civil Engineering, Harbin Institute of Technology, Harbin 150090, China; 18b933025@stu.hit.edu.cn (X.L.); tangliang@hit.edu.cn (L.T.); lingxianzhang@hit.edu.cn (X.L.)
[2] Heilongjiang Research Center for Rail Transit Engineering in Cold Regions, Harbin 150090, China
[3] Chongqing Research Institute, Harbin Institute of Technology, Chongqing 401135, China
* Correspondence: congshengyi@hit.edu.cn

Abstract: The term "engineering cancer" refers to expansive soil, whose properties threaten the stability and safety of structures. As a result, appropriate steps must be taken to guarantee the sustainable development of buildings. To explore the impact of freeze–thaw cycles (FTCs) on the microscopic characteristics of unsaturated expansive soil in the cold region, the mineralogical composition and microstructure were analyzed using X-ray diffraction (XRD), thermogravimetric analysis, and scanning electron microscopy (SEM). The influence of repeated FTCs on the characteristics of particle morphology and pore structure in expansive soil was quantitatively examined. The findings indicate that, in comparison to other expansive soil samples, the Yanji expansive soil is particularly susceptible to failures due to its high sand content and low liquid limit. The FTCs significantly alter the microstructure, leading to increased complexity in the particle edge shapes, a transition in particle distribution from dispersed to more concentrated, a reduction in larger particles, and a more intricate spatial arrangement of particles. As moisture content rises, the impact of FTCs becomes increasingly pronounced. The particle distribution's area probability index and fractal dimension are identified as medium-variability parameters, with a high-variation coefficient before the 3rd FTC, which then gradually decreases. The repeated FTCs result in particle breakage and agglomeration, causing the particle size to become more uniform and the soil's microstructure to stabilize after 3–5 FTCs. These findings contribute to understanding the FTC behavior of expansive soils, provide theoretical support and scientific guidance for disaster prevention and control measures, as well as for the sustainable development of engineering projects involving expansive soil sites.

Keywords: freeze–thaw cycle; unsaturated expansive soil; microstructure; pore characteristics

check for updates

Academic Editor: Syed Minhaj Saleem Kazmi

Received: 20 December 2024
Revised: 13 January 2025
Accepted: 17 January 2025
Published: 19 January 2025

Citation: Li, X.; Cong, S.; Tang, L.; Ling, X. Effect of Freeze–Thaw Cycles on the Microstructure Characteristics of Unsaturated Expansive Soil. *Sustainability* **2025**, *17*, 762. https://doi.org/10.3390/su17020762

Copyright: © 2025 by the authors. Licensee MDPI, Basel, Switzerland. This article is an open access article distributed under the terms and conditions of the Creative Commons Attribution (CC BY) license (https://creativecommons.org/licenses/by/4.0/).

1. Introduction

In engineering practice, expansive soil exhibits special deformation properties, namely, swelling and shrinking when in contact with water, repeated expansion and contraction, and a sharp attenuation of immersed bearing capacity, which cause great harm to the sustainable development of engineering construction [1]. These characteristics make it easy for roads to settle unevenly, for the roadbed slope to collapse, and for foundations and building structures to deform and crack [2]. Consequently, "engineering cancer" is another name for this [3]. However, expansive soil is widely distributed in China and abroad, mainly in Yunnan, Guangxi, Guizhou, Hubei, and other provinces in China, as well as in southeast Africa and southeast Asia [4–10]. In recent years, engineering practice has found that large-scale expansive soil sites frequently occur in seasonal frozen soil areas

such as Jilin, Liaoning, and Heilongjiang, and this has an important impact on engineering construction and the prevention of damage caused by freezing [11–14].

To effectively implement sustainable disaster prevention and control measures for expansive soil sites, it is essential to address the issue at its root. The special microstructure of expansive soil is the essential cause factor that induces geological disasters. Understanding the microstructure characteristics of expansive soil is the basis of studying its deformation behavior (Al-Rawas and McGown, 1999 [15]; Katti and Shanmugasundaram, 2001 [16]). Due to its special mineral composition and pore structure, unsaturated expansive soil is prone to significant volume change under the conditions of moisture and temperature changes [17–19]. During freeze–thaw cycles (FTCs), processes such as water migration, ice crystal formation, and subsequent melting result in dynamic alterations to the soil's microstructure, which in turn affect its mechanical properties. Lu and Liu [20] performed the apparent expansive soil cracking induced by FTCs. Li et al. [21] and Zhang et al. [22] studied the mechanisms affecting the bearing strength under FTCs, in terms of the CBR, of weakly expansive soil that could be used as embankment filler. Olgun [23] evaluated the geotechnical properties of an expansive soil subject to a freeze–thaw effect. Yu et al. [24] investigated the freezing characteristics of the expansive soil and the important factors affecting the freezing characteristic curve. Sun et al. [25] discussed the expression degree and influencing factors of the structural strength of expansive soil. Consequently, when investigating the cracking behavior of expansive soils in cold regions, it is essential to account for the impact of FTCs to mitigate potential project risks. Currently, while some researchers have investigated the mechanical behavior of unsaturated expansive soil under freeze–thaw action, most research has mainly focused on the macroscopic changes on the expansive soil site [26]; an in-depth exploration of the dynamic changes in the microstructure is lacking. Numerous researchers have carried out comprehensive analyses and studies on the impact of dry–wet cycles on expansive soil (Han et al., 2024 [27]; Zhao et al., 2021 [28]; Ding et al., 2021 [29]). The freeze–thaw cycle effect, as a powerful weathering process, has had a notable impact on the expansion behavior and crack formation in expansive soils in deep seasonally frozen regions in recent years. However, it is noteworthy that research on the coupling effects of moisture content and FTCs for unsaturated expansive soil has not been carried out in depth. In response to this, expansive soils from northeast China were chosen as the focus of the study. To address the demand for sustainable construction using expansive soil in northeast China, this study integrated local climatic conditions and geological characteristics and investigated the changes in the microscopic structure and the fracture characteristics of the expansive soil while considering the FTCs' action and moisture content. The research findings further elucidate the underlying causes of disaster-proneness at the Yanji expansive soil site and uncover the micro-mechanisms governing the effects of freeze–thaw cycles.

In this research, the FTC experiments and scanning electron microscope (SEM) analyses were conducted on unsaturated expansive soil with varying initial moisture contents. The primary goals of the study were (1) to examine the impact of FTCs on the morphology of unsaturated expansive soil particles; (2) to elucidate how initial moisture content and FTCs influence the spatial arrangement of the microstructure; and (3) to develop a micro-mechanism to explain the role of FTCs in engineering failures related to expansive soil. These findings contribute to understanding the FTC behavior of expansive soils, provide theoretical support and scientific guidance for disaster prevention and control measures, and enable the sustainable development of engineering projects involving expansive soil sites.

2. Test Materials and Methods

2.1. Basic Physical Properties of Soil

The expansive soil used in the experiments was sourced from the Yanji section of the Jilin–Tumen–Hunchun high-speed railway, a location representative of the region (Figure 1). The topography is mainly intermountain erosion hilly landform, and the groundwater is rich and mainly fissure water. The strata are mainly interbedded sandstone and mudstone of the upper Cretaceous Longjing Formation. The surface Quaternary Holocene residual slope silty clay is hard-plastic. The upper Cretaceous Longjing Formation sandstone and mudstone are interbedded. The rock is soft and the argillaceous cementation is poor. In its natural state, the soil is characterized by a hard-plastic state, with a natural moisture content of 19.17% and a dry density of 1.49 g/cm^3 (Figure 2). After air drying and grinding, using a 2 mm sieve, the large particles were removed from the expansive soil collected from the site. The basic physical properties of the soil are outlined in Table 1, with the grain size distribution shown in Figure 3, the compaction curve shown in Figure 4, and the proportions of each fraction presented in Table 2. The characteristic curve of soil and water was determined by the filter paper method, and the moisture content–suction relationship of expansive soil is shown in Figure 5. The free expansion rate test revealed that the soil's free swelling rate is 50%. According to the Code for Soil Test of Railway Engineering (TB 10102-2023; China's Ministry of Transport, 2023), this soil is classified as weak expansive soil and categorized as sandy fine-grained soil, a type of low liquid limit clay (CL-S).

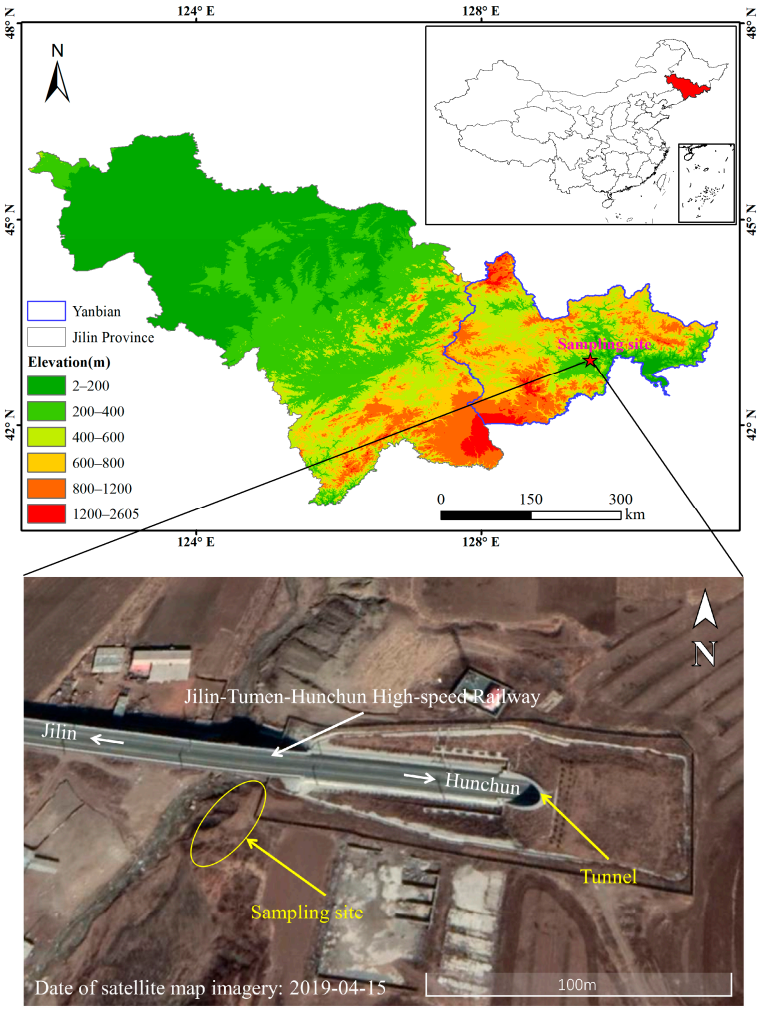

Figure 1. Sample site along the high-speed railway in Yanji.



Figure 2. Macroscopic characterization of expansive soil at the site.

Table 1. Physical properties of expansive soil.

Plastic Limit (%)	Liquid Limit (%)	Plasticity Index (%)	Optimum Moisture Content (%)	Maximum Dry Density (g/cm^3)	Free Swelling Ratio (%)
19.10	37.39	18.29	19.83	1.69	50

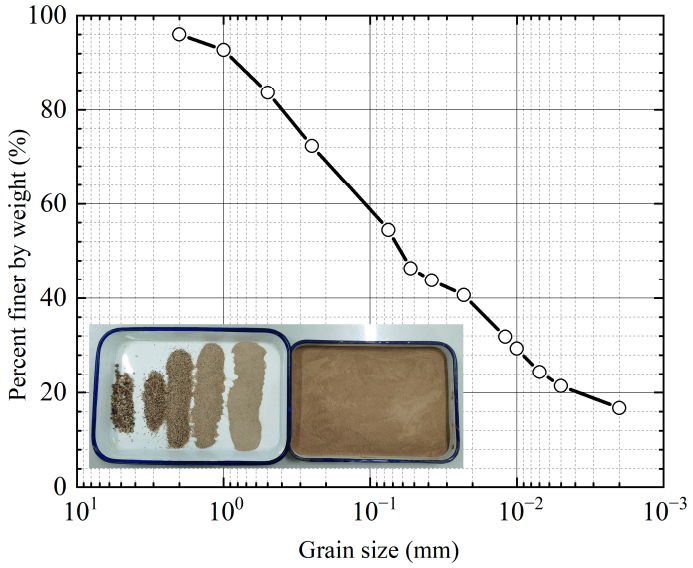

Figure 3. Grain-size distribution of expansive soil.

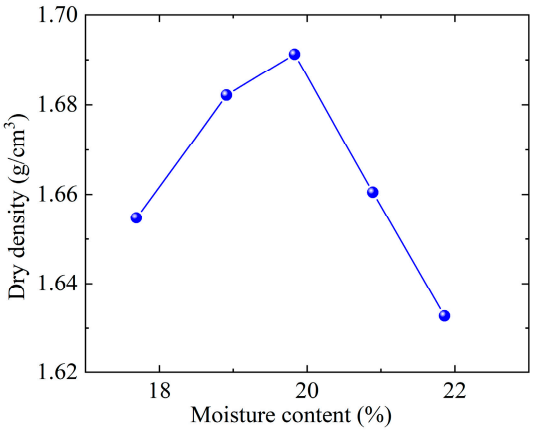

Figure 4. Compaction curve of expansive soil.

Table 2. Proportions of each fraction.

General Designation of Fraction	Fine Grain		Coarse Grain	
Name of fraction	Clay	Silt	Sand	Gravel
Particle size range (mm)	$d \leq 0.005$ mm	0.005 mm < $d \leq$ 0.075 mm	0.075 mm < $d \leq$ 2 mm	2 mm < $d \leq$ 20 mm
Proportion (%)	21.41	33.05	41.58	3.96

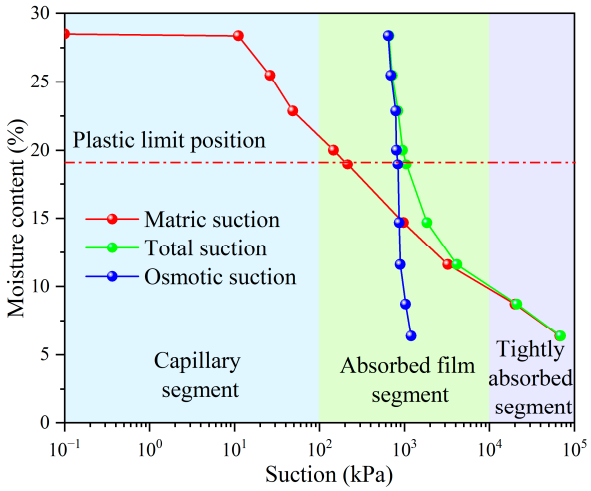

Figure 5. Soil–water characteristic curve of expansive soil.

2.2. Sample Preparation and Tests

X-ray diffraction (XRD) and thermogravimetric analyses were carried out on the undisturbed cutting ring sample from the site. The wet sieve analysis method was employed to separate the expansive soil particles into different size fractions, allowing for the examination of the micro-morphologies of the particles within these ranges after the agglomeration of the dispersed particles.

Microscopic observation samples were prepared to undergo different FTCs with different moisture content. The preparation method for a microstructure observation sample is as follows. Using the sample percussion method, cutting ring samples were prepared with dimensions of Φ39.1 mm × 80 mm. Microscale samples were then created, representing both untreated soil and soil subjected to varying FTCs. To ensure uniform expansion potential, the dry density of the samples was consistently controlled at 1.52 g/cm^3, and it was ensured that the compaction degree reached 90%. To prevent moisture loss, the prepared loose samples with different moisture contents were wrapped in plastic wrap and were maintained for one day before the FTC tests were conducted. The moisture content was controlled to 14% (Group X), 20% (Group Y), and 26% (Group Z), and the 20% condition was the condition closest to the optimum moisture content. According to the local climate conditions and the FTC test scheme used in a previous study [4], the FTC test was designed with a freezing temperature of −15 °C for 12 h, followed by a thawing temperature of 15 °C for 12 h. According to the previous research conducted by our research group [12], the number of freeze–thaw cycles (N_{FTC}) for each sample is set to five distinct FTCs (i.e., 0, 1, 3, 7, and 11 cycles). The samples were labeled based on the group letter and the N_{FTC}. For example, the sample name X11 indicates that the sample has a moisture content of 14% (Group X) and undergoes 11 FTCs.

Scanning electron microscopy was employed to examine the micro-morphology of the expansive soil. The sample was dried and gently broken along a shallow tank to expose the fresh structural surface of the soil sample. A relatively flat fracture surface was chosen for scanning observation, and a small SEM sample approximately 1 cm × 1 cm × 0.5

cm (length × width × height) was carefully cut using a sharp blade. Loose particles on the surface were gently removed with an ear bulb syringe. The sample surface was then coated with gold using an SBC-12 ion-sputtering device, and the gold-coated sample was transferred to the observation chamber for analysis. A Phenom Pro bench scanning electron microscope was used for the electron microscope scanning to avoid structural singularity of the soil samples, and photographs of a representative area were taken from high power to low power to obtain images of the microstructure. Images with a magnification of 1000× provided a clearer view of the overall microstructure, while images at 8000× magnification were used to analyze the local, representative microstructural characteristics of the particles.

2.3. Microscopic Image Analysis Methods

The particles (pores) and crack analysis system (PCAS) was employed for the quantitative microscopic image analysis [30]. The SEM images of the soil samples were imported, and the particles were automatically identified through binarization, with black as particles and white as pores (Figure 6b). The results after vectorization are shown in Figure 6c, and different colors represent different pores. Statistical parameters, including the average form factor, area–circumference fractal dimension, area probability distribution index, fractal dimension of the particle distribution, and probabilistic entropy were obtained via quantitative analysis, and the particle morphology, grain-size distribution, and arrangement were quantitatively analyzed. The pore characteristics were analyzed according to the pore classification after the PCAS analysis. Based on the microscopic study of the samples, the particles and pores belong to the same control system. According to the particle size classification standard, the pores in expansive soil can be categorized into four types [31]. The pore type of coarse pores ($d > 75$ μm) is inter-aggregate pores; the pore type of fine pores is inner-aggregate pores (5 μm $< d \leq 75$ μm); the pore type of micropores (0.1 μm $< d \leq 5$ μm) is inter-particle pores; and the pore type of ultramicropores ($d \leq 0.1$ μm) is inner-particle pores. The fine pores can be subdivided into three categories. The large pores (20 μm $< d \leq 75$ μm) consist of inter-aggregate pores and some inner-aggregate pores; the medium pores (10 μm $< d \leq 20$ μm) are inner-aggregate pores; and the small pores (5 μm $< d \leq 10$ μm) consist of inner-aggregate pores and some inter-particle pores (Table 3). According to the PCAS operation step [32], the obtained soil microscopic image was imported, and the threshold value was repeatedly adjusted until the particles in the pores were visible. The average value of the obtained threshold value for each of three measurements was utilized as the segmentation threshold in the segmentation program. Regarding the quantitative study of the particle characteristics, the following statistical parameters were calculated and analyzed to obtain more accurate quantitative relations.

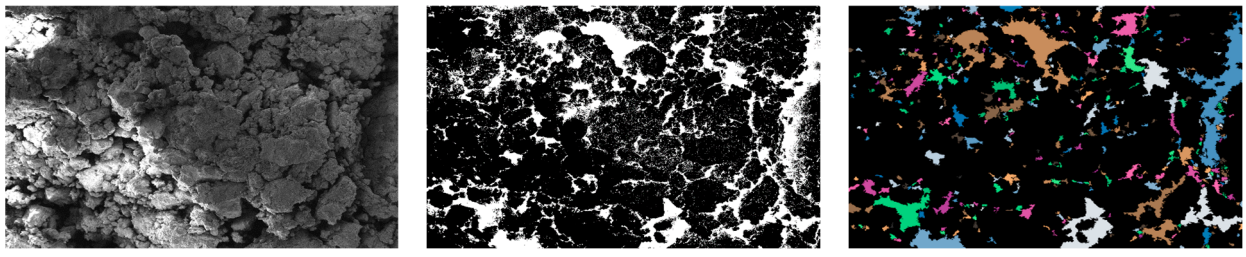

(**a**) (**b**) (**c**)

Figure 6. SEM image processing results: (**a**) Original image; (**b**) Binarization result; and (**c**) Vectorization result.

Table 3. Classification of pore types (after Ye et al., 2019 [31]).

Pore Type		Pore Size Range (μm)	Pore Composition
Coarse pores		d > 75 μm	Inter-aggregate pores
Fine pores	Large pores	20 μm < d ≤ 75 μm	Inter-aggregate pores and some inner-aggregate pores
	Medium pores	10 μm < d ≤ 20 μm	Inner-aggregate pores
	Small pores	5 μm < d ≤ 10 μm	Inner-aggregate pores and some inter-particle pores
Micropores		0.1 μm < d ≤ 5 μm	Inter-particle pores
Ultramicropores		d ≤ 0.1 μm	Inner-particle pores

(a). The average form factor $\overline{ff}$ of different particles in the same plane is used to describe the roundness of soil particles and the shape of particle edges. The closer the value is to 0, the rougher and more uneven the shape of particle edges;

(b). According to the fractal characteristics of the particle shape, the area-circumference fractal dimension D is between 1 and 2. The smaller the D value, the simpler the particle structure and the greater the degree of smoothness of surface of the spatial morphology of the particles;

(c). The area probability distribution index b represents the trend in particle count as the particle area increases, with the relationship between the two following a power function. A higher value of the area probability distribution index indicates a predominance of smaller particles and fewer larger ones;

(d). The fractal dimension of the particle distribution D_d characterizes the degree of particle homogenization and indicates the variability in particle size. A larger fractal dimension signifies poorer particle uniformity, a more concentrated distribution, and a higher degree of collectivization;

(e). The probabilistic entropy H_m is a parameter that reflects the arrangement of the particles. The value range of H_m is [0, 1]. A higher value indicates a more disordered particle arrangement, with lower levels of order.

3. Test Results and Analysis

3.1. XRD Results

The composition and structural morphology of the clay minerals was obtained via X-ray diffraction analysis (Figure 7). Based on the XRD analysis of the unsaturated expansive soil, the impact of these cycles on the material composition of the expansive soil from Yanji was investigated. The characteristic peaks of montmorillonite with a center of 6.03° (2θ) appear in the XRD patterns, and the diffraction peaks of the montmorillonite phase in the system decrease under the FTCs. The characteristic peaks of the albite phase appear between 26° and 30° (2θ). By comparing the characteristic peaks of albite after 0 and 11 FTCs, the diffraction intensity decreases. As the N_{FTC} increases, the diffraction peak intensity of quartz strengthens. The XRD analysis results indicate that the tested expansive soil from Yanji is mainly composed of montmorillonite, albite, quartz, potassium feldspar, illite, and hematite. After 11 FTCs, the XRD diffraction peak was shifted to the left at a small angle due to the increase in the lattice constant, which may be due to the change in the lattice constant caused by the doping of atoms. This can also be caused by lattice distortion. The contents of the various substances in the samples subjected to 0 and 11 FTCs are presented in Table 4. With increasing N_{FTC}, the contents of quartz, illite, and hematite increase, while the contents of montmorillonite, albite, and potassium feldspar decrease. The FTC exerts a form of frozen differentiation effect, which is more intense than the common physical differentiation effect and has a greater effect on the soil structure.

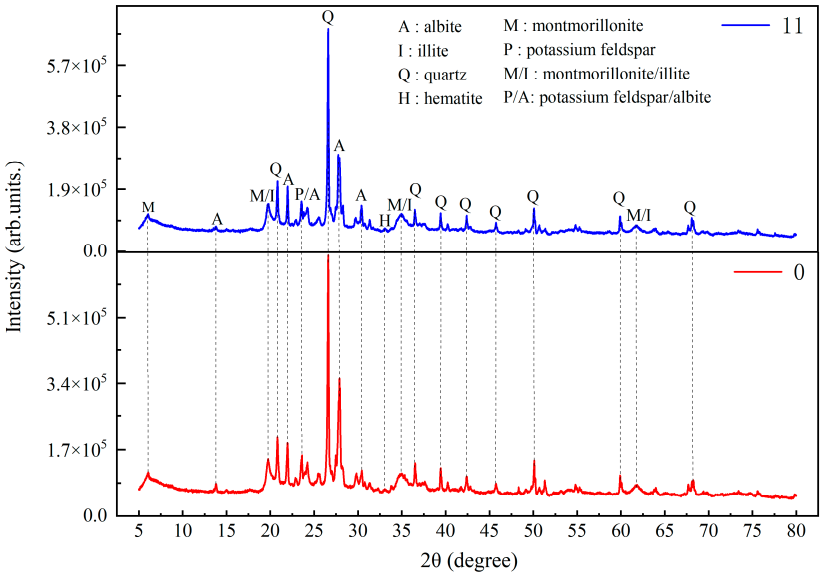

Figure 7. XRD patterns of expansive soil after 0 and 11 FTCs.

Table 4. Mineral compositions of the expansive soil based on XRD analysis results.

Sample	Montmorillonite (%)	Illite (%)	Albite (%)	Potassium Feldspar (%)	Quartz (%)	Hematite (%)
FT-0	51.9	2.8	26.4	3.8	14.9	0.2
FT-11	51	4	26	2	16	1

3.2. Thermogravimetric Analysis

The STA449F3 Jupiter synchronous thermal analyzer was utilized for thermogravimetric analysis of the samples, and two parallel measurements were carried out in this experiment. Finally, the thermogravimetric (TG)–derivative thermogravimetric (DTG) curves were obtained by measuring the temperature and weight loss during the experiment for mineral analysis.

As shown in Figure 8, the TG–DTG curve was derived from the temperature and weight loss measured from the thermogravimetric test data. The TG curve of the expansive soil shows that the amount of weight damage and the loss rate were greater after 11 FTCs, indicating that the damage effect of the lattice structure of the montmorillonite was more obvious. There are three obvious endothermic valleys in the DTG curve of the expansive soil. The first endothermic valley appears between 80 °C and 150 °C, and it is a compound valley. The second endothermic valley appears between 400 °C and 500 °C. The third endothermic valley is between 750 °C and 800 °C, and it is followed by an exothermic peak. The curves above demonstrate that montmorillonite is the predominant mineral in the expansive soil from Yanji. Furthermore, the first endothermal valley is a complex type of valley, which indicates that the montmorillonite is calcium-based montmorillonite. With increasing temperature, the free water in the sample first evaporated and absorbed heat, and a valley appeared in the TG curve at about 100 °C, which was combined to form the first composite endothermic valley. This was caused by the removal of the adsorbed water and interlayer water according to the distribution of the calcium montmorillonite. It can be seen from the temperature values marked in Figure 8 that the FTCs had a weak influence on the adsorbed water and interlayer water in the soil sample. The FTCs had minimal impact on the hydration capacity of the Ca^{2+}. The second endothermic valley appears near 430 °C. The crystal water was removed in this temperature zone, the original lattice was transformed, and the temperature values of the bottoms of the two curves were only

slightly different. The third endothermic valley is located within the temperature range of 750–800 °C. This valley exhibits a shallow shape, and the mass loss is relatively minor due to the lower content of structural water. The high temperatures in this range induced lattice damage, leading to the release of structural water and resulting in more or less irreversible changes within the structure. The subsequent exothermic peak indicates the formation of new phases, specifically, spinel and quartz. However, there is a large difference in the bottom temperature. After 11 FTCs, the temperature is higher compared to that of the untreated samples, with the valley shape becoming more pronounced. This indicates that the FTCs increased the content of the structural water in the soil samples and enhanced the stability of the microstructure. From the above analysis, it can be concluded that the FTCs resulted in great changes in the mineral composition and microstructure, which are mainly reflected in the decrease in the montmorillonite content and the weakening of the expansibility. The FTCs enhanced the structural thermal stability of the expansive soil and also amplified the weight loss characteristics and structural damage effects of the soil samples at high temperatures.

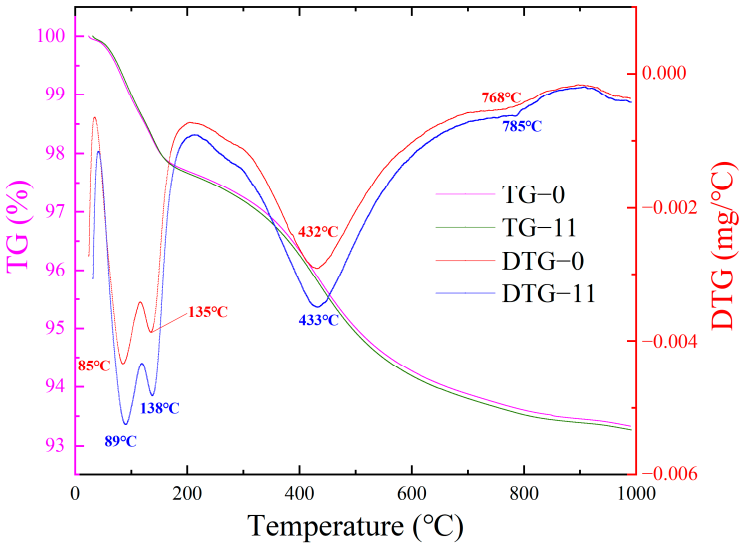

Figure 8. TG–DTG curves of the expansive soil after different N_{FTC}. Note: TG−0 and TG−11, DTG−0 and DTG−11 represent the TG curves and DTG curves of Yanji expansive soil samples with 0 and 11 FTCs, respectively.

3.3. Characteristics of Microstructure

3.3.1. Microscopic Characteristics of Particle Separation

For the soil sample utilized in this study, the silt content is 33.05% and sand content is 41.58%. These two components collectively form the skeletal structure of the expansive soil. The clay cements and encapsulates the single grains. The mineral composition is intricately linked to the particle size. Consequently, both the shape and structure of the soil particles vary according to their sizes. To further investigate the properties of the expansive soil particles, we conducted segmented analysis on the samples collected from Yanji according to the different particle size ranges. To ensure complete dispersion of these interbonded particles, wet sieve analysis was employed to separate them into distinct particle size fractions. The results of the expansive soil particle separation are shown in Figure 9, where Group A consists of soil particles above 1 mm-sieve; Group B consists of soil particles above 0.5 mm-sieve; Group C consists of soil particles above 0.25 mm-sieve; Group D consists of soil particles above 0.1 mm-sieve; Group E consists of soil particles above 0.075 mm-sieve; Group F consists of soil particles under 0.075 mm-sieve; and Group H is unclassified expansive soil particles.



(**a**) (**b**)

Figure 9. Particle separation results for the expansive soil: (**a**) Unclassified expansive soil; and (**b**) Expansive soil stored in tubes after separation. Note: Group A, B, C, D, E, F, and H represent different groups of expansive soil particles.

Figure 10 presents SEM images of the particles with different particle sizes. It can be seen that the dispersed particles are mainly subangular, debris and lamellar clay minerals are attached to their surfaces, and the colors within each particle size range are significantly different. According to the characteristics of the particles, the particles of the expansive soil from Yanji are more subangular, with a small amount of debris and lamellar clay minerals on their surfaces, and nano-pores are present locally [33]. There are pores and detrital complexes between the particles, and micron-level debris particles and clay minerals form aggregate particles.

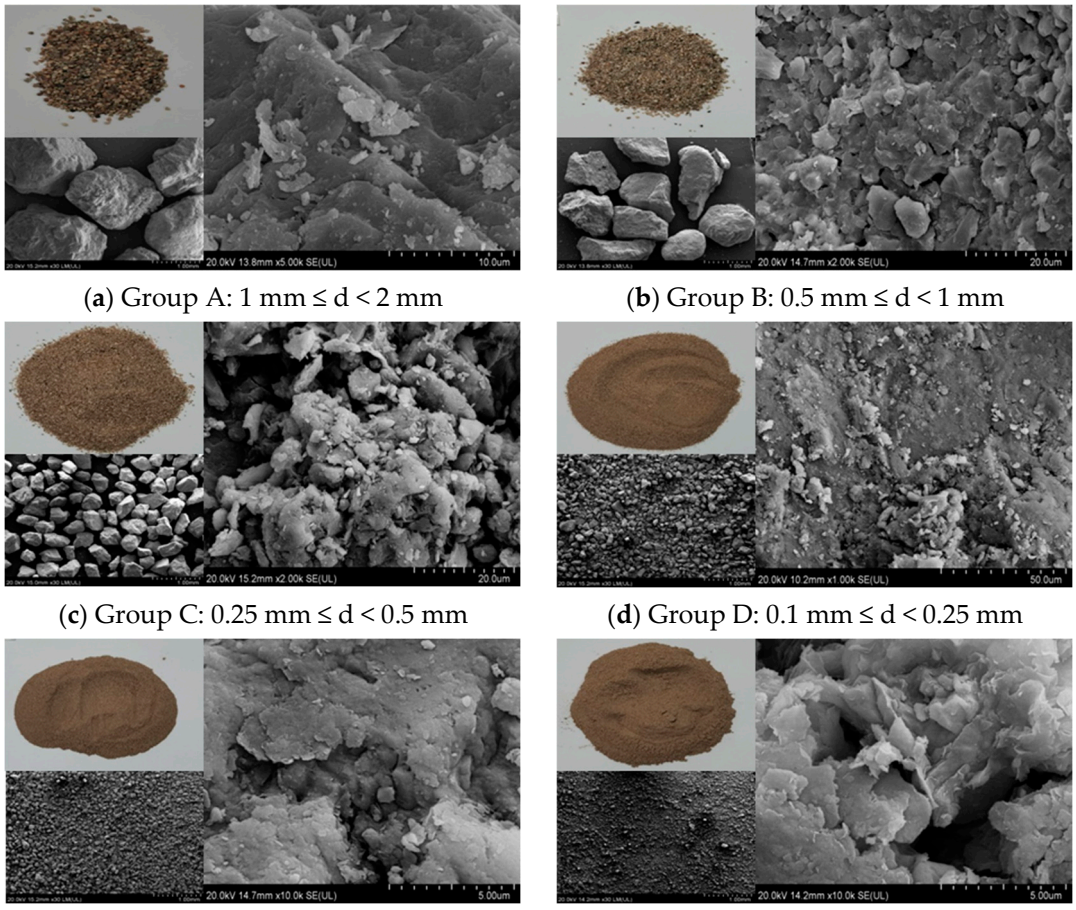

(**a**) Group A: 1 mm ≤ d < 2 mm (**b**) Group B: 0.5 mm ≤ d < 1 mm

(**c**) Group C: 0.25 mm ≤ d < 0.5 mm (**d**) Group D: 0.1 mm ≤ d < 0.25 mm

(**e**) Group E: 0.075 mm ≤ d < 0.1 mm (**f**) Group F: d < 0.075 mm

Figure 10. Characteristics of particles of different sizes in the expansive soil.

Since the Yanji expansive soil is a fine-grained soil with a sand content of as high as 41.58%, which constitutes the main soil skeleton of the expansive soil, a detailed analysis of the shape characteristics of the particles larger than 0.075 mm was essential. The basic geometric parameters of the particle shape calculated using image-processing software were used to calculate the near-sphericity, elongation, and equivalent diameter. The calculation results for all the particles were statistically calculated (Table 5). The average elongation is 0.57, indicating that the overall shape of the particles is inclined to be block shaped. The average near-sphericity of 0.33 is low, indicating that the surfaces of the particles have edges and that the shape of the particles is angular or subangular. The average roundness is 0.53, indicating a nearly rectangular shape. Therefore, we used a partial block shape, which is mainly subround or subangular, as the shape of the soil particles in the test.

Table 5. Statistics of the particle shape parameter calculation results.

	Maximum	Minimum	Range	Mean	Mid-Value
Elongation	0.95	0.13	0.79	0.51	0.57
Proximal sphericity	0.78	0.01	0.77	0.33	0.36
Roundness	0.93	0.16	0.87	0.53	0.47

3.3.2. Qualitative Analysis of Microscopic Characteristics

SEM was performed to examine the microstructure of expansive soil samples with varying moisture contents, subjected to different N_{FTC}. The microstructure image of the Group X expansive soil sample is shown as an example (Figure 11) to illustrate the microstructure characteristics of the expansive soil. It was observed that the N_{FTC} significantly influenced the arrangement and contact relationships of the expansive soil particles, thereby impacting the fractal characteristics of the microstructure. The SEM results revealed that the overall state was relatively stable after one FTC. After three FTCs, the signs of surface layer shedding were obvious and appeared within a wide range. After seven FTCs, in addition to some micro-cracks that began to cause material to fall off layer by layer, the cracks extended to a certain depth around the silt, and the cementation of the clay began to break down at this time. After 11 FTCs, the layered shedding still existed in a large area, the vertical penetration pores gradually deepened to form holes with a width of about 10 μm, and the horizontal penetration pores gradually became more abundant.

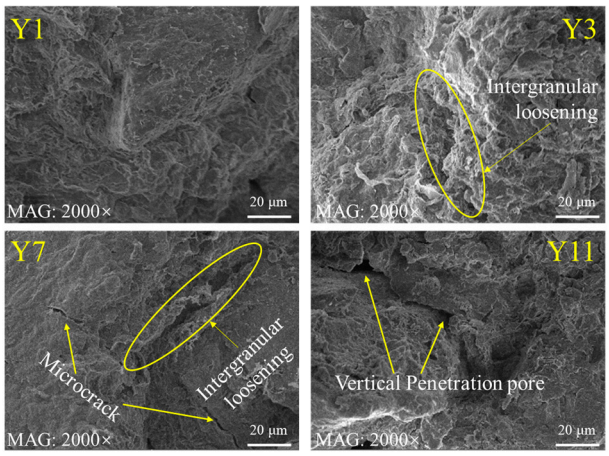

Figure 11. SEM images of the expansive soil after different N_{FTC}.

Expansive soils exhibit varying characteristics depending on the moisture content. When the natural moisture content approaches the plastic limit, the expansive soil is in a dry state and becomes hard and prone to cracking. Conversely, when this type of soil is saturated, its volume increases significantly with increasing moisture content,

demonstrating pronounced expansibility. The cracks may narrow or close as the soil structure becomes denser. As the moisture content decreases, the volume of the soil inevitably shrinks, leading to shrinkage phenomena and contraction stress. In this study, for the remolded expansive soil sample, the soils with different moisture contents also exhibited distinct characteristics (Figure 12). The microstructure of the low-moisture-content samples revealed that the clay particles initially aggregated around the sand or silt particles while still maintaining a flocculent structure. During the sample preparation, particle formation occurred due to compaction efforts. With increasing moisture content, the clay particles continued to aggregate. However, the Group Y samples achieved the most dense state. Additionally, more fragmentation cracks developed after the FTCs. In the Group X samples (i.e., a lower moisture content), the contacts between the particles remained relatively sparse. Consequently, numerous large pores persisted after compaction. In contrast, for the Group Z samples, after compaction, a more pronounced agglomeration phenomenon was observed in the dry soil mixed with water. This resulted in an increase in the presence of large pores and enhanced penetration pore development under FTC conditions.

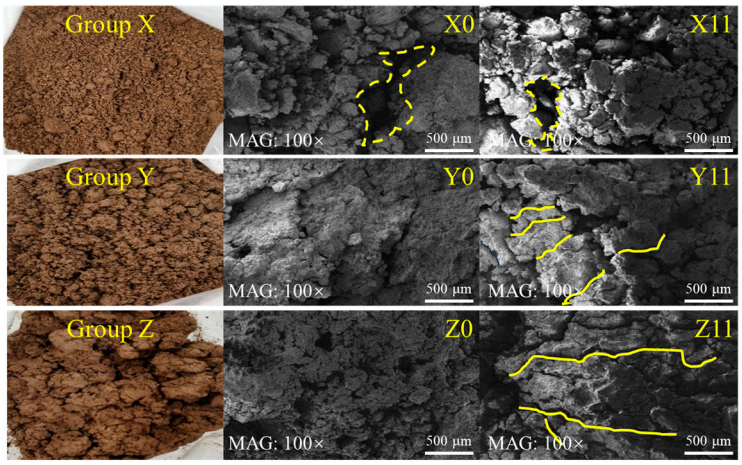

Figure 12. Microstructures of expansive soil samples with different moisture contents and N_{FTC}.

The morphologies of the soil particles of the expansive soil were observed under 2000× magnification (Figure 13), including granular and agglomerate types. The granular particles can be subdivided into subrounded, angular, strips, flaky, and mostly angular and flaky. The particle agglomerates can be subdivided into compositionary, accretionary and superimpositionary, and mainly compositionary and superimpositionary. The compositionary particle agglomerates were formed by the complete cementation of the small particles to the large particles, which belong to the outer clay-like particles. The accretionary particle agglomerates were formed by the accumulation of particles. Due to the large clay content of the expansive soil, the accumulation form is relatively small, and the accumulation is a weak zone. The superimpositionary particle agglomerates were formed in the form of edge–edge, edge–face, or face–face contacts with the flake particles. Overall, the structural unit of the expansive soil sample is largely composed of compositionary and superimpositionary particle agglomerates, and a clay particle matrix is present in these structures, thus forming irregular aggregates. Following Ye et al. [31], loess contains a relatively high percentage of silt and exhibits weaker cementation. In contrast, this study finds that the particles in expansive soil have a higher clay content and stronger cementation, resulting in a more closely connected arrangement and a more robust structure. Moreover, the lower the moisture content, the more pronounced this characteristic becomes. This observation

also explains why expansive soil was historically misidentified as a high-quality foundation material due to its high strength and low compressibility under drought conditions.

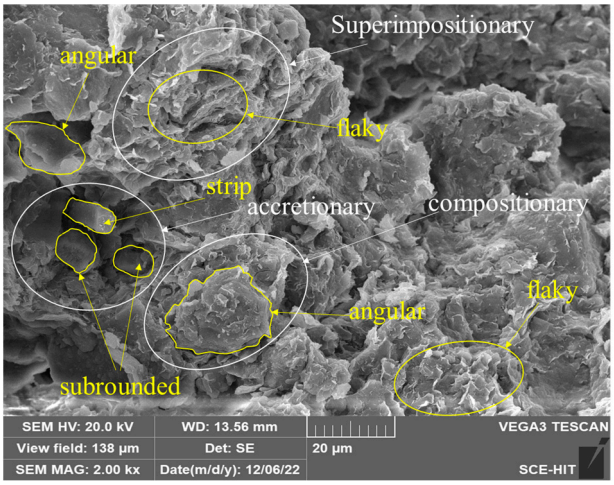

Figure 13. Microscopic features of the expansive soil sample.

3.3.3. Quantitative Analysis of Microscopic Characteristics

The quantitative analysis of the microstructure parameters was mainly carried out to assess the impact of the moisture content and the N_{FTC} on the morphology, grain-size distribution, and arrangement of the soil particles [30].

Figure 14a shows the variations in the average form factor, which decreases as the moisture content and N_{FTC} increase. The greater the moisture content, the greater the effect of the N_{FTC}. Under the action of FTCs, the particle edge shape tends to be complicated, and the collected grain shape tends to be irregular. Figure 14b shows the variations in the area–circumference fractal dimension o. As the moisture content and N_{FTC} increase, the area–circumference fractal dimension of the particles increases until it becomes stable. It can be seen that the complexity of the morphology of the skeleton particles increases as the N_{FTC} increases. Figure 14c shows the variations in the area probability distribution index with the N_{FTC}, and it increases as the N_{FTC} and moisture content increase. This indicates that the structural units with large areas decrease under the action of FTCs. With increasing moisture content, the adhesive effect of the clay particles is enhanced, and the structural units with large areas increase. Figure 14d shows the fractal dimension of the particle distribution. As the N_{FTC} increases, the fractal dimension of the particle distribution increases. With increasing moisture content, the fractal dimension of the particle distribution gradually decreases. Under the strong physical weathering caused by FTCs, large particles are broken due to the effect of the freezing of the water in the soil, and the homogenization and concentration of the particles are enhanced. Figure 14e shows the probabilistic entropy, which initially increases and then decreases as the N_{FTC} increases. It also increases with increasing moisture content. After the FTCs, it is evident that the particle arrangement changes from chaotic to ordered, with three FTCs marking a turning point. It is challenging for the particle distribution to achieve a uniform state during the compaction process because the bonding effect between the particles is increased by the increase in moisture content.

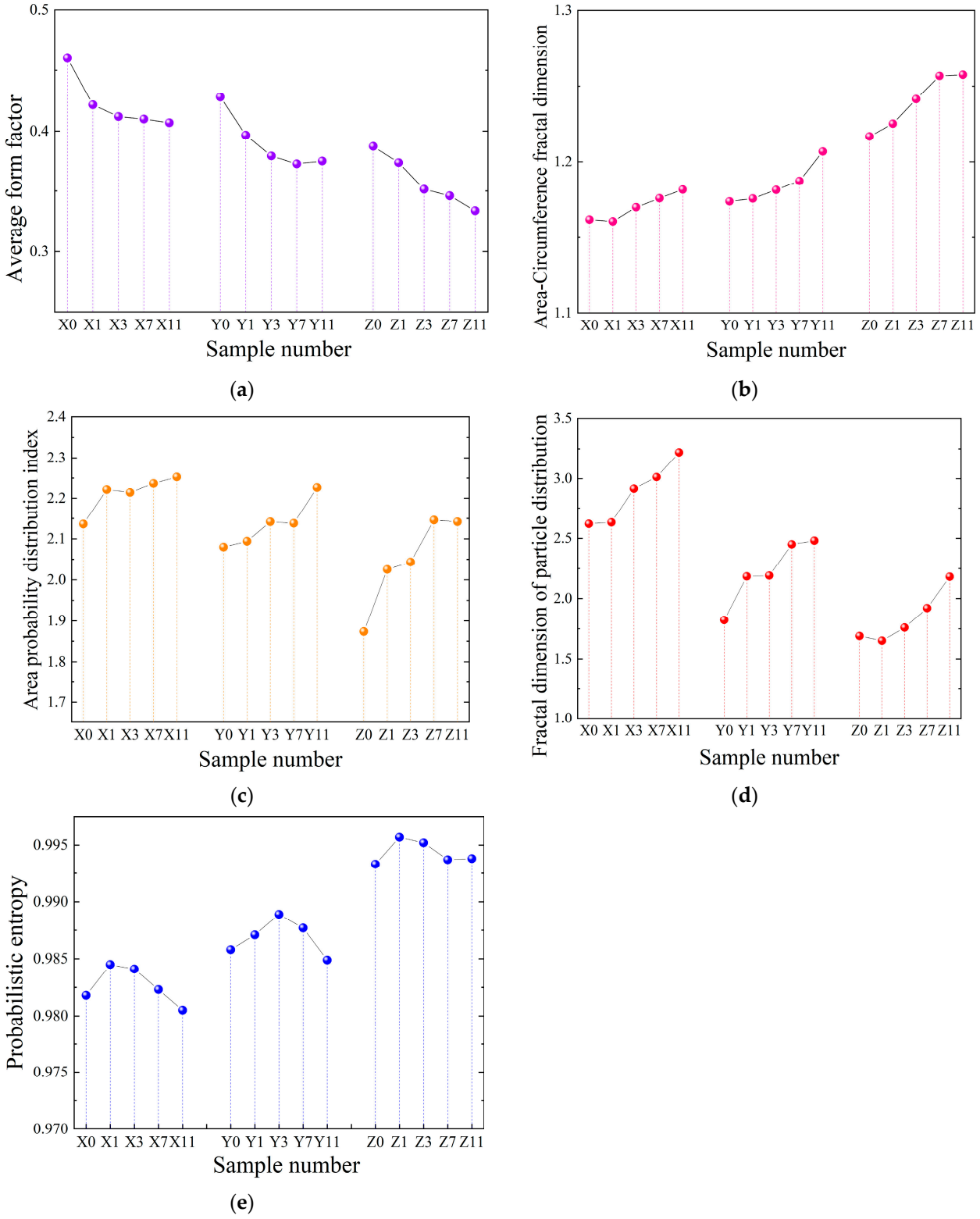

Figure 14. Microscopic characteristics of the expansive soil samples: (**a**) Average form factor; (**b**) Area–circumference fractal dimension; (**c**) Area probability distribution index; (**d**) Fractal dimension of particle distribution; and (**e**) Probabilistic entropy.

To visualize the changes in the characteristics of the different types of pore distributions after FTCs, the PCAS V2.3 software was used to calculate the classified pore characteristics. According to Table 3, the pores can be divided into coarse pores (d > 75 μm), large pores (20 μm < d ≤ 75 μm), medium pores (10 μm < d ≤ 20 μm), small pores (5 μm < d ≤ 10 μm),

micropores (0.1 μm < d ≤ 5 μm), and ultramicropores (d ≤ 0.1 μm). A stacked bar plot of the pore classification area ratio changes is shown in Figure 15, and the changes in the fractal dimension are shown in Figure 16.

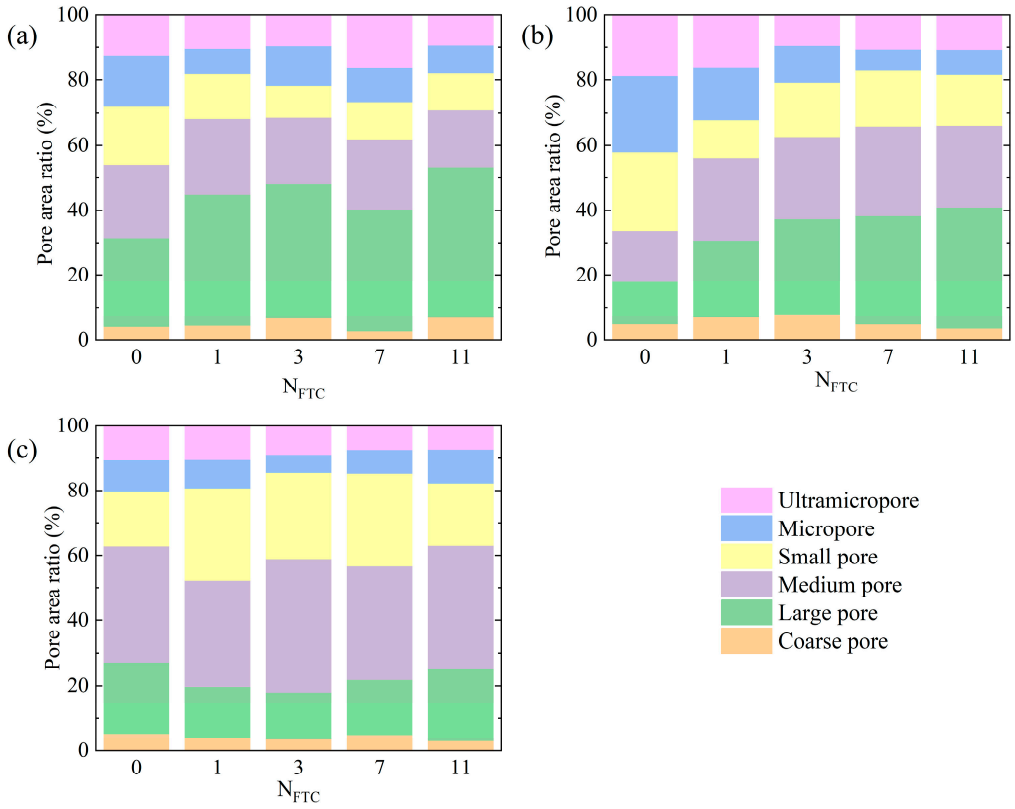

Figure 15. Pore area ratio of the expansive soil samples: (**a**) Moisture content of 14%; (**b**) Moisture content of 20%; and (**c**) Moisture content of 26%.

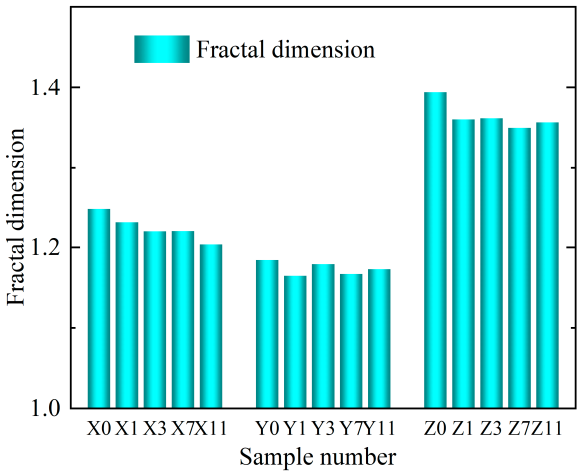

Figure 16. Variations in pore fractal dimension for the samples.

For the moisture content of 14% (Figure 15a), the influence of the FTCs on the different pore types was dynamic and persistent, and the proportion of each pore type fluctuated to a certain extent under different N_{FTC}. In particular, the proportions of the coarse pores and ultramicropores changed greatly, while the proportion of the fine pores increased significantly after the first FTC and then gradually stabilized. The proportion of the large pores exhibited an increasing trend in general. For the moisture content of 20% (Figure 15b), the coarse pores fluctuated significantly during the FTCs, initially increasing

and then decreasing. The large pores increased continuously. The medium pores fluctuated greatly during the FTCs. The small pores also fluctuated greatly during the FTCs, but they tended to decrease in general. In general, the number of fine pores increased gradually during the FTCs. The micropores and ultramicropores tended to decrease in general. For the moisture content of 26% (Figure 15c), the proportions of the coarse pores and ultramicropores decreased after multiple FTCs. The proportion of the pores of each category of fine pores fluctuated, and that of the large pores initially decreased and then increased. Generally speaking, the percentages of small and medium pores rose in the early stages and marginally declined in the later stages. There was a general upward trend in the percentage of micropores, which decreased in the early stages and rebounded in the latter stages.

Figure 16 shows the variations in the pore fractal dimension with N_{FTC}. As the N_{FTC} increased, the pore fractal dimension varied slightly but generally dropped, suggesting that the pore structure's complexity reduced. Overall, the fractal dimensions of the samples with low moisture contents and high moisture contents decreased significantly with increasing N_{FTC}, indicating that the pore structure of these samples became more uniform or less porous during the FTCs. The fractal dimension of the optimal moisture content sample changed little, indicating that its structure was relatively stable during the FTCs. The findings demonstrate that the effect of the FTCs was evident and that the cementation of the samples with low moisture levels was poor as a result of their low water content. The FTCs had a bigger effect on samples with higher moisture levels because of the increased moisture content. As a result, the FTCs had a greater influence in the beginning stage and stability in the later stage. The FTCs had the least impact on the sample with the optimum moisture level, which also had a more compact structure and higher cementation strength.

4. Discussion

4.1. Effect of Freeze–Thaw Cycles on Microstructure

The variability of the microscopic characteristics of the expansive soil under the action of FTCs needs to be combined with the FTC and parameter changes before and after the FTCs, so the two parameters of the amount of change and the coefficient of variation are introduced. The formula for calculating the amount of change is

$$\Delta M = B_n - A, \tag{1}$$

where ΔM is the variations in the property parameters during the FTCs; B_n is the parameter values of the material properties after FTCs; A is the parameter values of the material properties that have not experienced FTC; and n is the N_{FTC}. ΔM is the difference in the corresponding index under the action of the different FTCs. If $\Delta M > 0$, the corresponding index value increases; otherwise, the index value decreases.

The formula for calculating the coefficient of variation K is

$$K = \frac{1}{n}|A - B|, \tag{2}$$

where K is the coefficient of variation, that is, the frequency and severity of the changes in the various indicators under FTC, which can be used to judge the strengths of the changes in the various indicators under FTC. When $0 \leq K \leq 0.1$, the variability is low. When $0.1 \leq K \leq 1$, the variability is medium. When $K > 1$, the variability is high.

The changes in the microscopic characteristics of the expansive soil samples with different moisture contents and subjected to different N_{FTC} are shown in Figure 17, in which the changes in the average form factor were negative, indicating that the FTCs increased the complexity of the particle edge shapes. The changes in the area–circumference

fractal dimension, area probability distribution index, and fractal dimension of the particle distribution were positive, indicating that the number of large particles decreased, the spatial morphology of the particles became complicated, and the particle distribution changed from dispersed to concentrated under the FTCs. The variation characteristics of the above four indexes all indicate that, the greater the moisture content, the more significant the effect of the FTCs. With increasing N_{FTC}, the change in the probabilistic entropy gradually decreased from positive to negative, indicating that, compared with the samples not subjected to FTCs, those subjected to FTCs initially exhibited an increase and then a decrease in the probabilistic entropy index. Moreover, the probabilistic entropy values of the group X and group Y samples were lower than those of the no-FTCs samples, indicating that the particle arrangement's order declined and that it became chaotic under the FTCs. The occurrence of multiple FTCs formed new connections and structures inside the soil samples. Under the fragmentation and agglomeration of the soil particles, the grain size homogenized, and eventually the changes in the soil samples' characteristics progressively stabilized and established a new equilibrium.

Based on the above analysis, the coefficient of variation was introduced to analyze the degrees of change of the quantitative indexes of the particles during the FTC process (Figure 18). The statistical parameters of microstructure particles can be used to quantitatively analyze the characteristics of particle morphology, arrangement, and grain-size distribution, among which the average form factor and area–circumference fractal dimension were used to represent the morphological characteristics, area probability distribution index and fractal dimension of the particle distribution were used to represent the grain-size distribution characteristics, and the probabilistic entropy was used to represent the arrangement characteristics. According to the classification criteria for the variability, although the average form factor, area–circumference fractal dimension, and probability entropy changed during the FTCs, the variability was small, indicating that these were low-variability parameters. The variabilities of the area probability distribution index and the fractal dimension of the particle distribution were medium. Their coefficients of variation were large before the third FTC, and then the variability gradually decreased. The medium variation level indicates that the FTC mainly had a great influence on the particle grain-size distribution in the expansive soil sample, which is also consistent with the conclusion of Zhang et al. [34]. Due to the decreasing effects of the soil particle arrangement structure and grain-size distribution changes (i.e., the decreases in the degrees of these changes), the fluctuation frequency of the coefficients of variation decreased, which also indicates that the soil sample formed a new stable structure after several FTCs. In essence, the coefficients of variation of these physical properties were also closely related to the changes in the structure, particle size composition, and mineral composition of the soil, and the internal changes in the sample were reflected by the various coefficients of variation, so they can be used to analyze the mechanical properties of the sample to a certain extent.

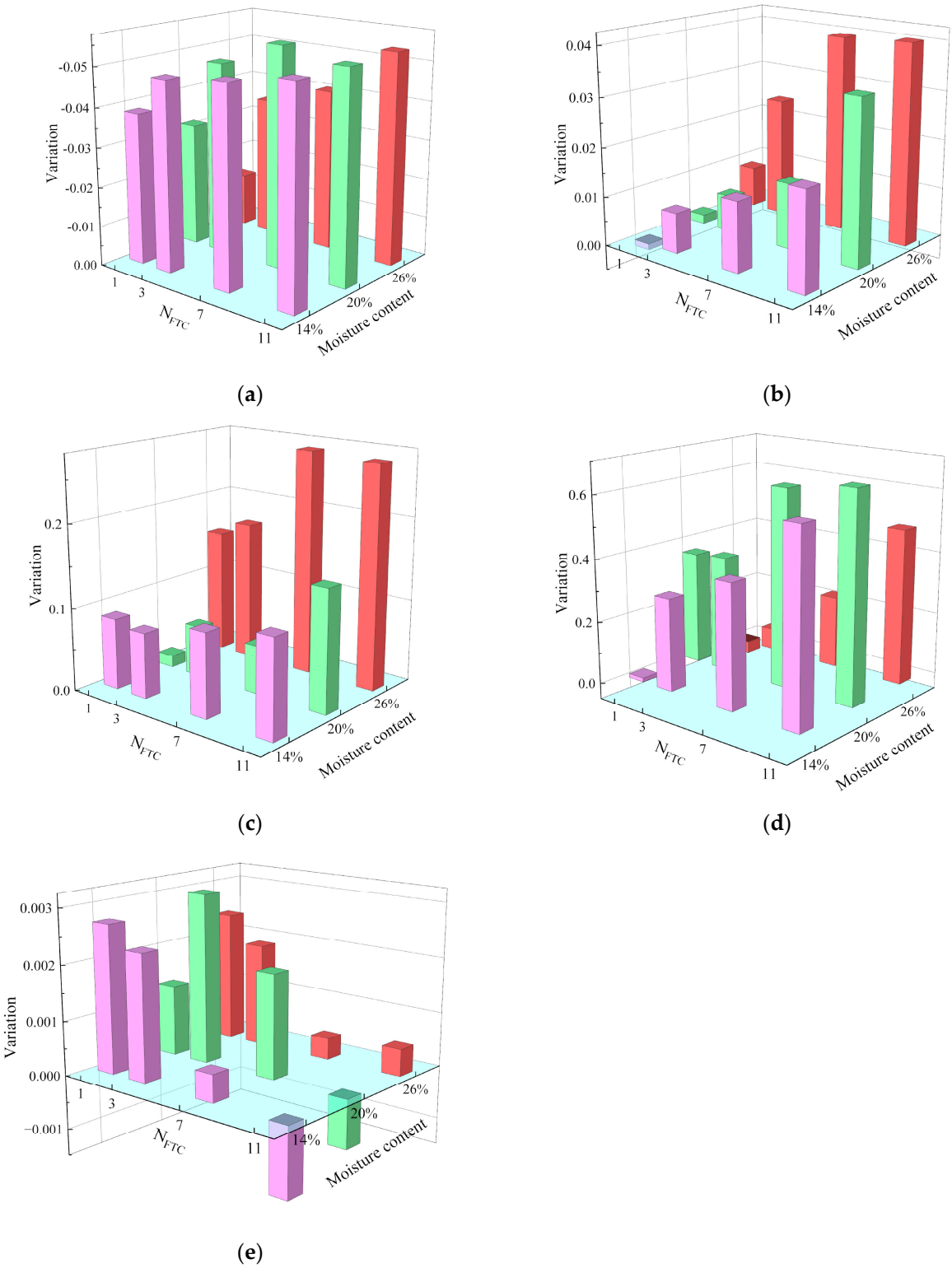

Figure 17. Variations in the quantitative indexes for the expansive soil particles: (**a**) Average form factor; (**b**) Area–circumference fractal dimension; (**c**) Area probability distribution index; (**d**) Fractal dimension of the particle distribution; and (**e**) Probabilistic entropy. Note: The purple, green, and red in this bar chart represent the results of groups X, Y, and Z, respectively.

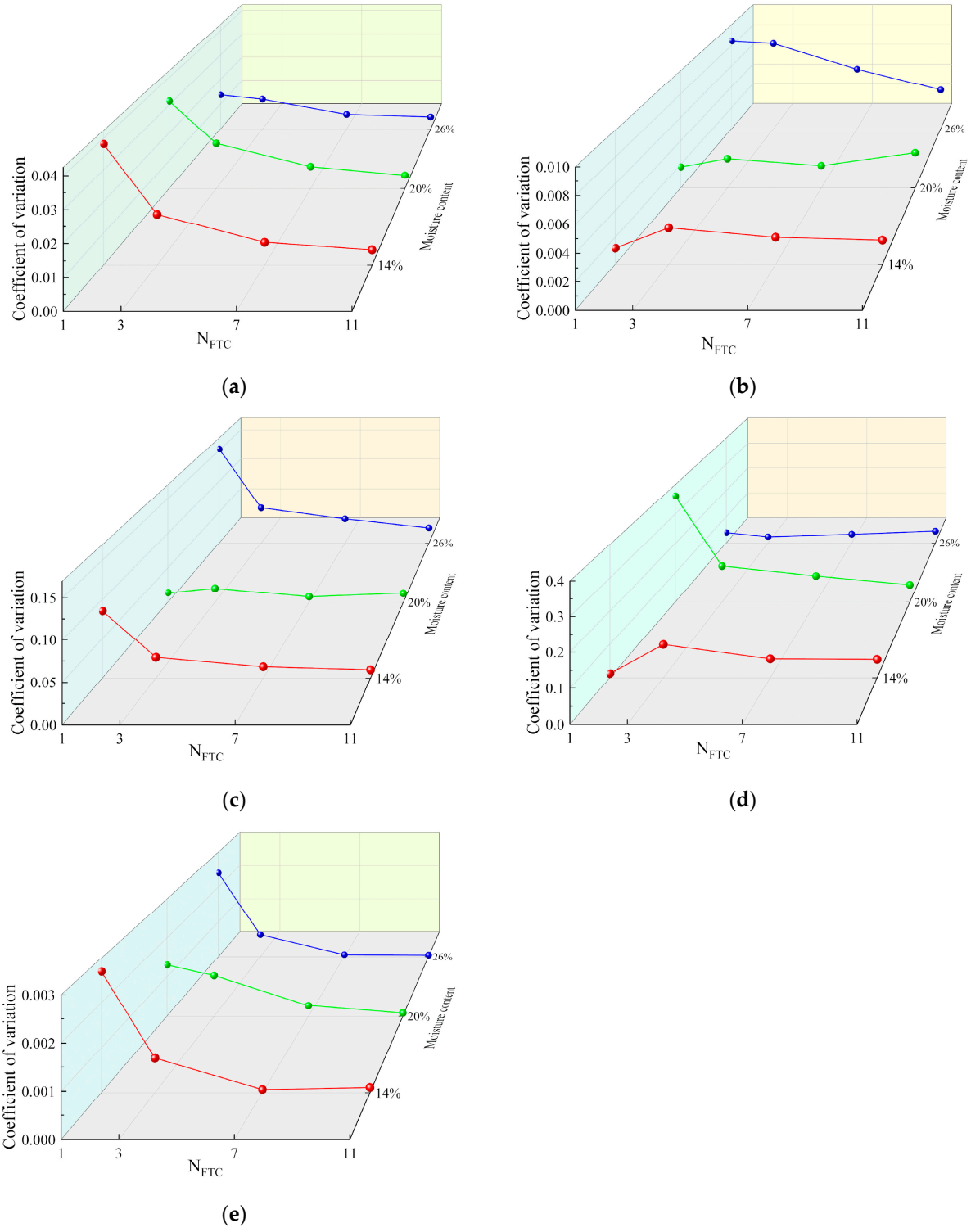

Figure 18. Coefficients of variation of the quantitative indexes of the expansive soil particles: (**a**) Average form factor; (**b**) Area–circumference fractal dimension; (**c**) Area probability distribution index; (**d**) Fractal dimension of the particle distribution; and (**e**) Probabilistic entropy. Note: The red, green, and blue in this line chart represent the results of groups X, Y, and Z, respectively.

4.2. Mechanism of Freeze–Thaw Action in Unsaturated Expansive Soil

The FTCs process leads to the splitting of coarse-grained particles and the agglomeration of fine-grained particles, which occur synchronously. Repeated FTCs cause the soil particles to break or agglomerate, thus changing the size of the particles. The fragmentation and agglomeration of particles not only change the size of the particles but also

change the morphology of the particles. The changes in the particle morphology result in changes in the soil mechanical properties. After several FTCs, the composition of the soil will have greatly changed. The mineral particles with larger grain sizes will fragment, while the smaller particles will agglomerate. After this, the changes in the particle size of the entire sample exhibit a decreasing trend, and the whole particle size composition evolves toward uniformity. The changes in the composition cause changes in the structural connections between the particles. During the freezing process, the structural connections of the soil particles change from condensation to condensation-agglomeration to crystallization. The changes in the soil structure during the FTCs also produce different integrated, network, or layered structures due to the FTCs. The FTC test revealed that, during the first and second freezing steps, the soil bodies were divided into layers of different sizes by ice interlayers, and they recovered their original overall structure after melting occurred (Figure 19). In the subsequent 3–5 FTCs, the structure was completely integrated, and the phenomenon in which the layers and integrated structure occurred alternately during the FTC process no longer occurred [34,35]. Many scholars have analyzed the influence of freeze–thaw cycles on the macroscopic mechanical characteristics of expansive soil [4,12,14]. The research shows that the freeze–thaw effect will have a certain weakening effect on the mechanical characteristics, and, when the number of freeze–thaw cycles exceeds a certain value, the strength and creep characteristics of expansive soil will tend to be stable. From the perspective of engineering practice, the characteristics of shallow destruction, easy disintegration, and low residual strength of expansive soil indicate that the expansive soil site has a high probability of significant damage in the first spring thawing period after disturbance, and will stabilize after several freeze–thaw cycles. In this study, the damage mechanism of an expansive soil site is studied comprehensively from the microscopic level. The summarized research work will be useful when designing corresponding mitigation measures for expansive soil sites in seasonally frozen regions.

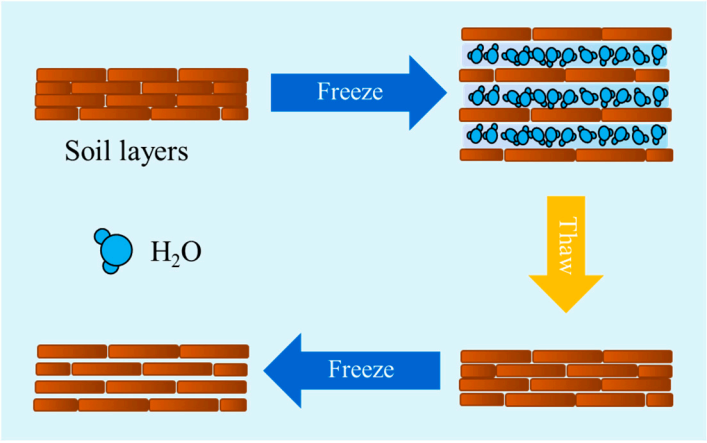

Figure 19. Schematic diagram of the changes in the expansive soil layer structure during the FTCs process (after Zhang et al., 2013; Zhan et al., 2019) [34,35].

Akagawa et al. [36] and Lai et al. [37] concluded that, when the macroscopic crystallization stress exceeds the tensile strength of the soil, the pore structure will be destroyed and cracks will form. The heat and moisture exchange during FTCs causes considerable changes in the pore, disrupting the arrangement and connection of the soil particles. In this study, FTCs significantly influence the arrangement mode and contact relationships of expansive soil particles, thereby affecting the fractal characteristics of the microstructure. Micro-cracks form in the water dissipation channel during FTCs. With increasing N_{FTC}, the number and scale of the micro-cracks increase. The contact mode of the microstructure particles gradually develops into point–edge contacts and edge–surface contacts, and

the arrangement mode of the microstructure particles is mostly void structure. With an increasing N_{FTC}, cracks develop in the coarse particles, while the agglomeration of fine particles becomes more pronounced. The particles that constitute the skeleton of the sample are more broken, and the amounts of floc and clay substances at the contacts and surface of the particles increase. We found that the large pores gradually changed into small pores, the accretionary and superimpositionary particle agglomerates gradually dissipated, compositionary-dominated particle agglomerates formed, and the particles became more tightly arranged, with the primary contact form being face-to-face. After several FTCs, the particles of the group X samples remained relatively intact and the particle surfaces were relatively clean. Most of the structural units were composed of silty particles in contact with one another. With increasing moisture content, the effect of the FTCs on the samples was significant [38]. The particles became more fragmented, and the clay particles aggregated and wrapped around the surfaces of the silt, forming a silt–clay aggregate (Figure 20). In Figure 20, the "wet" group represents the expansive soil sample whose moisture content is higher than the optimum moisture content, the "optimum" group represents the expansive soil sample with the optimum moisture content, and the "dry" group represents the expansive soil sample whose moisture content is lower than the optimal moisture content.

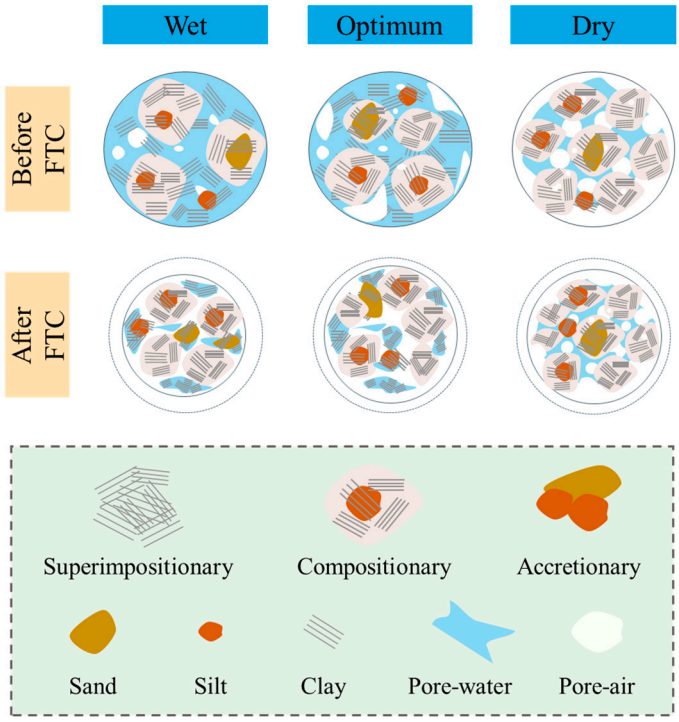

Figure 20. Schematic diagram of the microstructure changes under FTCs (after Wei et al., 2024) [38].

5. Conclusions

The physical properties and microstructure evolution of expansive soil under FTCs were studied, and the quantitative indexes of particle and pore microstructure characteristics of expansive soil under FTCs were analyzed. The effects of FTCs on the material composition, mineral particles, and microstructure of expansive soil were measured comprehensively, and the effects of FTCs and moisture content on expansive soil were explained from the microscopic point of view. The main conclusions are summarized below:

(1) Compared with other expansive soil sections, the expansive soil section in Yanji is prone to disasters because the soil has a high sand content and low liquid limit. The expansive soil particles of the samples from Yanji are partially blocky particles, which are mainly subrounded or subangular. Under the influence of FTCs, the structural

thermal stability was enhanced, the expansion was weakened, and the FTCs amplified the weight loss characteristics of and structural damage effects on the soil samples at high temperatures;

(2) For the remolded expansive soil sample, the soils with different moisture contents also exhibited distinct characteristics, and, the greater the moisture content, the more significant the effect of the FTCs;

(3) The FTCs increased the complexity of the particle edge shape, changed the particle distribution from dispersed to concentrated, decreased the proportion of large particles, and caused the spatial morphological characteristics of the particles to become more complicated. The variabilities of the area probability distribution index and the fractal dimension of the particle distribution were medium, and their coefficients of variation were large before the 3rd FTC; then, their variabilities gradually decreased;

(4) After the FTCs, the original structure of the soil particles was disrupted, leading to the formation of a new structure. Repeated FTCs caused the expansive soil particles to break and agglomerate, resulting in a more uniform particle size. Following three to five FTCs, the soil microstructure stabilized.

Author Contributions: Conceptualization, X.L. (Xinyu Li); Investigation, S.C.; Methodology, X.L. (Xinyu Li), S.C., L.T. and X.L. (Xianzhang Ling); Writing—original draft, X.L. (Xinyu Li); Writing—review and editing, S.C. All authors have read and agreed to the published version of the manuscript.

Funding: This research was supported by the Natural Science Foundation of Heilongjiang Province (LH2022E072), National Natural Science Foundation of China (Grant No. 42101125), the Open Research Fund Program of State Key Laboratory of Frozen Soil Engineering of China (Grant No. SKLFSE202015).

Institutional Review Board Statement: Not applicable.

Informed Consent Statement: Not applicable.

Data Availability Statement: The data presented in this study are available from the corresponding author upon request.

Conflicts of Interest: The authors declare no conflicts of interest.

Glossary

Symbol	Description
FTC	Freeze–thaw cycle
N_{FTC}	Number of freeze–thaw cycles
XRD	X-ray diffraction
SEM	Scanning electron microscopy
TG	Thermogravimetric
DTG	Derivative thermogravimetric
PCAS	Particles (pores) and crack analysis system
$\overline{ff}$	The average form factor
D	The area–circumference fractal dimension
b	The area probability distribution index
D_d	The fractal dimension of the particle distribution
H_m	The probabilistic entropy
ΔM	Variations in the property parameters during the FTCs
B_n	Parameter values of the material properties after FTCs
A	Parameter values of the material properties without FTC
n	N_{FTC} in the calculation formula
K	The coefficient of variation

References

1. Chen, F.H. *Foundations on Expansive Soils*; Elsevier: Amsterdam, The Netherlands, 2012.
2. Nayak, N.V.; Christensen, R.W. Swelling characteristics of compacted expansive soils. *Clays Clay Miner.* **1971**, *19*, 251–261. [CrossRef]
3. Luo, P.; Ma, M. Failure Mechanisms and Protection Measures for Expansive Soil Slopes: A Review. *Sustainability* **2024**, *16*, 5127. [CrossRef]
4. Cong, S.Y.; Nie, Z.; Li, X.Y.; Tang, L.; Ling, X.Z.; Hu, Q.L.; Li, G.Y. Prediction of compressive creep behaviors of expansive soil exposed to freeze-thaw cycle using a disturbed state concept-based model. *Cold Reg. Sci. Technol.* **2022**, *204*, 103664. [CrossRef]
5. Ito, M.; Azam, S. Relation between flow through and volumetric changes in natural expansive soils. *Eng. Geol.* **2020**, *279*, 105885. [CrossRef]
6. Khemissa, M.; Mekki, L.; Mahamedi, A. Laboratory investigation on the behaviour of an overconsolidated expansive clay in intact and compacted states. *Transp. Geotech.* **2018**, *14*, 157–168. [CrossRef]
7. Kyokawa, H. A double structure model for hydro-mechano-chemical behavior of expansive soils based on the surface phenomena of mineral crystals. *Eng. Geol.* **2021**, *294*, 106366. [CrossRef]
8. Zhang, X.; Huang, T.; Wu, Y. Soil drainage clogging mechanism under vacuum preloading: A review. *Transp. Geotech.* **2024**, *45*, 101178. [CrossRef]
9. Yan, J.B.; Kong, L.W.; Wang, J.T. Evolution law of small strain shear modulus of expansive soil: From a damage perspective. *Eng. Geol.* **2023**, *315*, 107017. [CrossRef]
10. Zhang, F.; Cui, Y.J. Microstructure-based insight into different swelling pressure determination methods. *Eng. Geol.* **2022**, *307*, 106777. [CrossRef]
11. Zou, W.L.; Ding, L.Q.; Han, Z.; Wang, X.Q. Effects of freeze-thaw cycles on the moisture sensitivity of a compacted clay. *Eng. Geol.* **2020**, *278*, 105832. [CrossRef]
12. Tang, L.; Cong, S.; Ling, X.; Xing, W.; Nie, Z. A unified formulation of stress-strain relations considering micro-damage for expansive soils exposed to freeze-thaw cycles. *Cold Reg. Sci. Technol.* **2018**, *153*, 164–171. [CrossRef]
13. Zhang, X.; Ye, P.; Wu, Y.; Zhai, E. Experimental study on simultaneous heat-water-salt migration of bare soil subjected to evaporation. *J. Hydrol.* **2022**, *609*, 127710. [CrossRef]
14. Tang, L.; Cong, S.; Geng, L.; Ling, X.; Gan, F. The effect of freeze-thaw cycling on the mechanical properties of expansive soils. *Cold Reg. Sci. Technol.* **2018**, *145*, 197–207. [CrossRef]
15. Al-Rawas, A.A.; McGown, A. Microstructure of Omani expansive soils. *Can. Geotech. J.* **1999**, *36*, 272–290. [CrossRef]
16. Katti, D.R.; Shanmugasundaram, V. Influence of swelling on the microstructure of expansive clays. *Can. Geotech. J.* **2001**, *38*, 175–182. [CrossRef]
17. Basma, A.A.; Al-Homoud, A.S.; Husein, A. Laboratory assessment of swelling pressure of expansive soils. *Appl. Clay Sci.* **1995**, *9*, 355–368. [CrossRef]
18. Zhang, X.; Du, D.; Man, T.; Ge, Z.; Huppert, H. Particle clogging mechanisms in hyporheic exchange with coupled lattice Boltzmann discrete element simulations. *Phys. Fluids* **2024**, *36*, 013312. [CrossRef]
19. Sharma, R.S. *Mechanical Behaviour of Unsaturated Highly Expansive Clays*; University of Oxford: Oxford, UK, 1998.
20. Lu, Y.; Liu, S. Cracking in an expansive soil under freeze-thaw cycles. *Sci. Cold Arid Reg.* **2017**, *9*, 392–397.
21. Li, T.; Kong, L.; Liu, B. The California Bearing Ratio and Pore Structure Characteristics of Weakly Expansive Soil in Frozen Areas. *Appl. Sci.* **2020**, *10*, 7576. [CrossRef]
22. Zhang, X.; Huang, T.; Ge, Z.; Man, T.; Huppert, H.E. Infiltration characteristics of slurries in porous media based on the coupled Lattice-Boltzmann discrete element method. *Comput. Geotech.* **2025**, *177*, 106865. [CrossRef]
23. Olgun, M. The effects and optimization of additives for expansive clays under freeze-thaw conditions. *Cold Reg. Sci. Technol.* **2013**, *93*, 36–46. [CrossRef]
24. Yu, H.; Hao, F.; Yi, P.; Zhang, Q.; Ma, T. Experimental Investigation on the Effect of Salt Solution on the Soil Freezing Characteristic Curve for Expansive Soils. *Sustainability* **2024**, *16*, 363. [CrossRef]
25. Sun, X.; Song, S.; Niu, C.; Zhang, X.; Dou, C.; Xia, W.; Li, X.; Wang, Q. Investigation of the Structural Strength of Expansive Soil in a Seasonally Frozen Region. *Buildings* **2024**, *14*, 789. [CrossRef]
26. Yang, Z.; Lv, J.; Shi, W.; Jia, C.; Wang, C.; Hong, Y.; Ling, X. Experimental study of the freeze thaw characteristics of expansive soil slope models with different initial moisture contents. *Sci. Rep.* **2021**, *11*, 23177. [CrossRef] [PubMed]
27. Han, L.; Ji, W.; Ma, L.; Guo, R.; Zhang, Y.; Zhang, H. Microscopic Mechanisms and Evolution Models of Crack Development in an Expansive Soil under Conditions of Rainfall Evaporation Cycles. *Sustainability* **2024**, *16*, 7617. [CrossRef]
28. Zhao, G.T.; Han, Z.; Zou, W.L.; Wang, X.Q. Evolution of mechanical behaviours of an expansive soil during drying-wetting, freeze-thaw, and drying-wetting-freeze-thaw cycles. *Bull. Eng. Geol. Environ.* **2021**, *80*, 8109–8121. [CrossRef]
29. Ding, L.Q.; Vanapalli, S.K.; Zou, W.L.; Han, Z.; Wang, X.Q. Freeze-thaw and wetting-drying effects on the hydromechanical behavior of a stabilized expansive soil. *Constr. Build. Mater.* **2021**, *275*, 122162. [CrossRef]

30. Liu, C.; Shi, B.; Zhou, J.; Tang, C. Quantification and characterization of microporosity by image processing, geometric measurement and statistical methods: Application on SEM images of clay materials. *Appl. Clay Sci.* **2011**, *54*, 97–106. [CrossRef]
31. Ye, W.; Li, C. The consequences of changes in the structure of loess as a result of cyclic freezing and thawing. *Bull. Eng. Geol. Environ.* **2019**, *78*, 2125–2138. [CrossRef]
32. Liu, C.; Tang, C.; Shi, B.; Suo, W. Automatic quantification of crack patterns by image processing. *Comput. Geosci.* **2013**, *57*, 77–80. [CrossRef]
33. Liu, X.Y.; Zhang, X.W.; Kong, L.W.; Wang, G.; Li, C.S. Multiscale structural characterizations of anisotropic natural granite residual soil. *Can. Geotech. J.* **2023**, *60*, 1383–1400. [CrossRef]
34. Zhang, Z.; Ma, W.; Qi, J.L. Structure evolution and mechanism of engineering properties change of soils under effect of freeze-thaw cycle. *J. Jilin Univ. Earth Sci. Ed.* **2013**, *43*, 1904–1914. (In Chinese)
35. Zhan, J.W.; Wang, Q.; Zhang, W.; Shangguan, Y.L.; Song, S.Y.; Chen, J.P. Soil-engineering properties and failure mechanisms of shallow landslides in soft-rock materials. *Catena* **2019**, *181*, 104093. [CrossRef]
36. Akagawa, S.; Nishisato, K. Tensile strength of frozen soil in the temperature range of the frozen fringe. *Cold Reg. Sci. Technol.* **2009**, *57*, 13–22. [CrossRef]
37. Lai, Y.M.; Wu, D.Y.; Zhang, M.Y. Crystallization deformation of a saline soil during freezing and thawing processes. *Appl. Therm. Eng.* **2017**, *120*, 463–473. [CrossRef]
38. Wei, Y.; Tang, C.S.; Zhu, C.; Cheng, Q.; Lu, Y.; Li, L.; Tian, B.G.; Shi, B. Influence of desiccation during freeze-thaw cycles on volumetric shrinkage and tensile strength of compacted clayey soils. *Eng. Geol.* **2024**, *334*, 107513. [CrossRef]

Disclaimer/Publisher's Note: The statements, opinions and data contained in all publications are solely those of the individual author(s) and contributor(s) and not of MDPI and/or the editor(s). MDPI and/or the editor(s) disclaim responsibility for any injury to people or property resulting from any ideas, methods, instructions or products referred to in the content.